pubs.acs.org/Biomac

Article

Understanding Self-Assembly and Molecular Packing in Methylcellulose Aqueous Solutions Using Multiscale Modeling and Simulations

Zijie Wu, Audrey M. Collins, and Arthi Jayaraman*

Cite This: *Biomacromolecules* 2024, 25, 1682−1695

Read Online

ACCESS | Metrics & More | Article Recommendations | Supporting Information

ABSTRACT: We present a multiscale molecular dynamics (MD) simulation study on self-assembly in methylcellulose (MC) aqueous solutions. First, using MD simulations with a new coarse-grained (CG) model of MC chains in implicit water, we establish how the MC chains self-assemble to form fibrils and fibrillar networks and elucidate the MC chains' packing within the assembled fibrils. The CG model for MC is extended from a previously developed model for unsubstituted cellulose and captures the directionality of H-bonding interactions between the −OH groups. The choice and placement of the CG beads within each monomer facilitates explicit modeling of the exact degree and position of methoxy substitutions in the monomers along the MC chain. CG MD simulations show that with increasing hydrophobic effect and/or increasing H-bonding strength, the commercial MC chains (with degree of methoxy substitution, DS, ∼1.8) assemble from a random dispersed configuration into fibrils. The assembled fibrils exhibit consistent fibril diameters regardless of the molecular weight and concentration of MC chains, in agreement with past experiments. Most MC chains' axes are aligned with the fibril axis, and some MC chains exhibit twisted conformations in the fibril. To understand the molecular driving force for the twist, we conduct atomistic simulations of MC chains preassembled in fibrils (without any chain twists) in explicit water at 300 and 348 K. These atomistic simulations also show that at DS = 1.8, MC chains adopt twisted conformations, with these twists being more prominent at higher temperatures, likely as a result of shielding of hydrophobic methyl groups from water. For MC chains with varying DS, at 348 K, atomistic simulations show a nonmonotonic effect of DS on water-monomer contacts. For 0.0 < DS < 0.6, the MC monomers have more water contacts than at DS = 0.0 or DS > 0.6, suggesting that with few methoxy substitutions, the MC chains are effectively hydrophilic, letting the water molecules diffuse into the fibril to participate in H-bonds with the MC chains' remaining −OH groups. At DS > 0.6, the MC monomers become increasingly hydrophobic, as seen by decreasing water contacts around each monomer. We conclude based on the atomistic observations that MC chains with lower degrees of substitutions (DS ≤ 0.6) should exhibit solubility in water over broader temperature ranges than DS ∼ 1.8 chains.

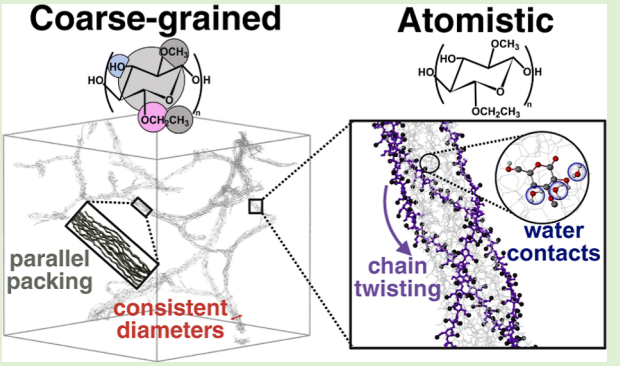

1. INTRODUCTION

Methylcellulose (MC), one of the most common cellulose derivatives, is widely used in a range of consumer products (e.g., as food additives, gelators, laxatives).[1−3] In MC chains, the hydroxyl groups (−OH) on each monomer are substituted by methoxy ($-OCH_3$) groups, and depending on the average number of substitutions per monomer, the degree of substitution (DS) of MC can vary from 0 (unsubstituted) to 3 (all three hydroxyl groups are converted to methoxy groups). At the molecular level, the substitution of −OH with $-OCH_3$ disrupts the interchain hydrogen bonding and alters the solubility of MC in both aqueous and organic solvents.[2] How soluble the MC chains are in aqueous and organic solvents is directly related to the DS and the randomness of substitution along the chain. Most common substitution procedures render a random methylation in terms of both the −OH positions (C2, C3, or C6) and the monomers along the chain; this is commonly referred to as the "heterogeneous" substitution pattern.[2,4] For such heterogeneous substitution, past studies have found that MCs with DS > 2.5 are soluble only in organic solvent because of the high hydrophobicity of the chains[5] and MCs with intermediate DS between 1.3 and 2.5, including the commercially available MC (DS of 1.7−2.0), are soluble in water at room temperature.[2,6,7]

Received: November 4, 2023
Revised: February 12, 2024
Accepted: February 12, 2024
Published: February 28, 2024

https://doi.org/10.1021/acs.biomac.3c01209
Biomacromolecules 2024, 25, 1682−1695

Besides DS, temperature also plays a key role in dictating the solubility and phase behavior of MC aqueous solutions. Commercially available MCs with DS between 1.7 and 2.0 have been shown to undergo thermoreversible gelation in water,[8] phase separating into a turbid gel above ∼50 °C.[9] Such gel formation and disassociation are thermally tunable and reversible, making MC gels useful for biomedical applications that require a thermoresponsive function (e.g., in tissue engineering[10−12] and drug delivery[13]). While the gelation temperature (T_{gel}) is known to be dependent on factors such as heating rate,[14] MC concentration, salt concentration,[15] and molecular weight,[16,17] the phase-separated structure has been found to be remarkably consistent after the gelation occurs. Microscopy and small-angle scattering experiments confirm that above T_{gel}, MC chains self-assemble into fibrils and fibrillar networks.[17,18] MCs' fibrillar networks exhibit desirable mechanical and rheological properties that make them useful as self-healing materials,[19] thickeners,[2] emulsifiers,[20] and stabilizers.[21] The wide commercial usage of MC solutions and gels motivates the need for understanding their structure and phase behavior.

In TEM images, the fibrillar aggregates of MC exhibit both densely packed, highly crystalline regions and loosely packed, low crystallinity regions; the densely packed, highly crystalline regions have smaller diameters than the relatively more amorphous regions.[22] Structural characterization of MC aqueous solutions through small-angle X-ray scattering (SAXS) shows that MC fibrils have a consistent fibril diameter with varying MC concentrations and molecular weights;[17] however, the molecular underpinnings of this observation remain unclear. To address this knowledge gap, we have used top-down (specifically, machine-learning-enhanced computational reverse engineering analysis of scattering experiments, ML-CREASE)[23] and bottom-up (molecular dynamics simulations[24]) computations; the latter is the focus of this paper. In the top-down approach,[23] using ML-CREASE and analytical model fits of SAXS profiles obtained by Lodge, Bates, and coworkers,[17] we confirmed that MC fibrils have consistent average diameters in the range of 17−20 nm at various MC concentrations and molecular weights. However, such a top-down approach does not describe the molecular packing within the fibrils or the molecular interactions that give rise to the consistent fibril diameters. To better understand the temperature-induced MC chains' assembly into these network structures with consistent fibril diameters, there is a need for a molecular perspective for the MC chains' assembly mechanism. Such a molecular insight has been difficult to obtain with direct imaging/microscopic techniques such as transmission electron microscopy (TEM) and cryo-EM.[22] This motivates our work in this paper using multiscale modeling and simulations that help us understand the role of relevant molecular interactions that drive MC chains to assemble into fibrils.

Past molecular modeling and simulation studies on MC solutions[25−29] have not been able to explain the assembly mechanism of MC chains into fibrils correctly because the selected model either missed relevant interactions or could not enable simulations at appropriate time scales and length scales of assembly. The monomer unit of MC can be considered as a hydrophobic cyclic acetal consisting of mainly carbon atoms with hydroxyl groups [hydrophilic (−OH groups) when unsubstituted and hydrophobic ($-OCH_3$ groups) when substituted]. In aqueous solutions of MC chains, there are two relevant interactions—one, hydrogen bonds between hydroxyl groups-hydroxyl groups and between water and some of the remaining hydroxyl groups, and two, hydrophobicity due to hexapyranose rings in MC chains' backbone and substituted methyl groups. These interactions and their relative contributions at various temperatures dictate the overall enthalpic and entropic gains/losses and resulting in free energy change associated with the assembly of MC chains from a dispersed, unassembled solution state. The significance of each of these interactions at various temperatures and degrees of methoxy substitution in MC chains is not intuitive or not easy to measure in experiments, justifying the need for simulations. While atomistic simulations of MC chains and explicit solvent molecules represent all relevant chemical details at the atomic level, they cannot capture time scales and length scales of macromolecular assembly of MC chains into fibrils from any random initial configuration. This is because the computational cost of atomistic simulations is too high to simulate the assembly of multiple polymer chains from a disordered initial configuration to an ordered configuration.[24,30,31] In most cases where atomistic simulations are necessary, one has to start the simulations with a preassembled initial configuration either known from experimental measurements (e.g., NMR or X-ray crystallography) or with an assumed structure of the MC chains in a preassembled fibril; for MC, the latter is the question these simulations are supposed to answer. As a result, atomistic simulations are often only used to compare the relative dominance of thermodynamic factors (such as hydrogen bonding effect at different temperatures in ref 27) or to derive the force field for the coarse-grained (CG) model of MC.[26] Alternatively, one may use CG models informed by the atomistic structure of MC or from experimental measurements of MC chains to reduce the computational cost and enable self-assembly without prior knowledge/assumption of assembled structure albeit with reduced chemical accuracy. Using CG molecular dynamics (MD) simulations, Huang et al. suggested that a single MC chain self-collapses into a ring/toroid structure, which might be a precursor of the final fibril structure.[26] With a similar CG approach, Ginzburg et al.[25] then explored the possibilities of multiple such rings stacking to form fibrils. A similar ring structure was also later observed and proposed in the CG modeling study by Li et al.[29] and Sethuraman and Dorfman,[28] who also proposed that such rings stack on top of each other to form the observed MC fibrils. The theory of MC fibril formation by ring stacking can explain the origin of consistent fibril diameter at different chain molecular weights and/or concentrations, as the diameter of the fibril would be determined by the diameter of the ring, which could, in turn, be dictated by the persistence length of the chain.[1,26] However, this "stacking toroid" model is not able to reconcile with key experimentally observed features of MC fibrils, including the correlation between chain contour length and fibril length[17] and the findings from medium-angle X-ray scattering/wide-angle X-ray scattering (WAXS) measurements that the individual MC chains are oriented along the fibril axis.[22] Therefore, based on existing experimental evidence, the most plausible explanation for the internal packing of MC fibril packing is that MC chains aggregate length wise, and most chains are aligned/are parallel to the fibril's long axis.[17,22] Supporting this aligned packing hypothesis from experiments, computational studies show generic self-attractive polymers (not specifically modeling MC) forming bundled fibrils of

https://doi.org/10.1021/acs.biomac.3c01209
Biomacromolecules 2024, 25, 1682−1695

finite diameter by parallel/aligned stacking,[32−34] with individual chains twisting along the fibril axis.

To the best of our knowledge, there have not been any CG models informed by atomistic structure of MC that simultaneously reproduce (1) formation of fibrils by aligned stacking of extended MC chains and (2) consistent fibril diameters with varying MC chain lengths (i.e., molecular weight) and concentration. In this paper, we address this knowledge gap by developing a CG model for MC chains informed by the atomistic structure of cellulose monomers[35] and then simulate the self-assembly of these chains from random configurations into MC fibrils in the implicit solvent, without any prior assumptions of how the chains could assemble. We then use these CG MD simulation-generated assembly structures as starting configurations for atomistic simulations to understand the explicit role of water around the MC chains.

2. COMPUTATIONAL METHODS

2.1. CG Modeling and Simulation. *2.1.1. Model.* The CG model for MC (Figure 1a) is extended from our previously developed

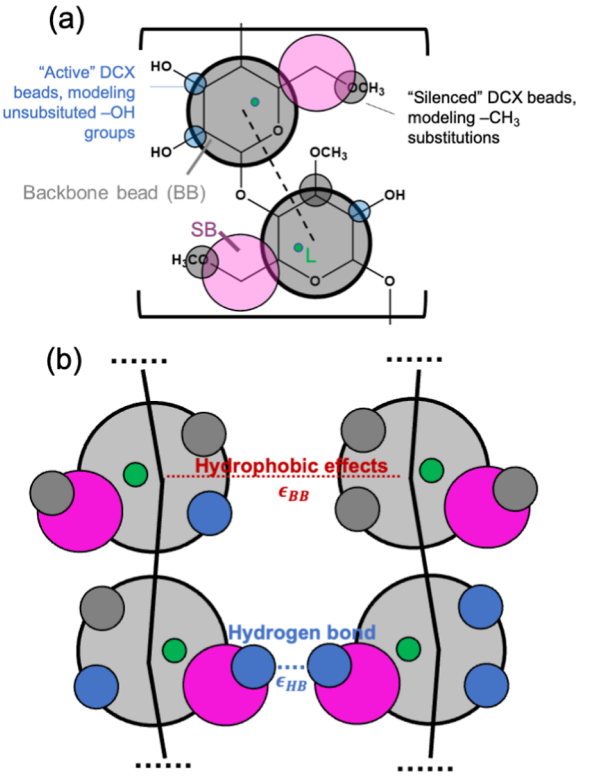

Figure 1. Schematics of (a) CG representation for two connected MC monomers and (b) nonbonded interactions modeling the hydrophobic effect and hydrogen bonding effect.

model for (unsubstituted) cellulose.[35] It represents each anhydroglucose unit (AGU) as a group of 6 CG beads: a backbone bead (BB) representing the carbon ring of AGU, a satellite bead (SB) representing the hydroxymethyl (C6−OH) group, a linker bead (L) serving as a connection point for the applied angle and dihedral potentials, and three hydrogen bonding beads (DC*X*, where *X* = 2, 3, or 6 corresponding to the numbering of connected carbon) representing the hydroxyl (−OH) groups. The BB bead has a diameter of 1*d*, where *d* is the reduced unit of length and roughly equal to 0.53 Å. The SB bead is of diameter 0.74*d* and the three DC*X* beads, when not substituted by a methyl group, are each of diameter 0.2*d* (shown in blue in Figure 1a). When a DC*X* bead is substituted, we refer to the DC*X* bead as "silenced" because the $-OCH_3$ it represents would be unable to hydrogen bond like the −OH, and we increase the DC*X* bead's diameter to 0.3*d* to qualitatively capture the increased steric hindrance of the $-OCH_3$ as compared to −OH. We refer to the unsubstituted DC*X* as "active" to contrast it from the "silenced" substituted DC*X* bead.

The bonded interactions (i.e., bond, angle, and dihedral potentials) between various pairs or groups of bonded beads along the MC chain are the same as the bonded interactions that we used in the cellulose CG model. Table S1 in the Supporting Information has more details about these interactions; for the rationale behind these selected bonded potentials we direct the readers to our previous work.[35]

The nonbonded interactions are chosen to capture the hydrogen bonding interactions and hydrophobic interactions between the MC chains' CG beads.

We model hydrogen bonding interactions between "active" DC*X* beads with a 12−6 Lennard-Jones (LJ) potential[36] as in eq 1

$$U_{HB}(r) = 4\epsilon_{HB}\left[\left(\frac{\sigma_{HB}}{r}\right)^{12} - \left(\frac{\sigma_{HB}}{r}\right)^{6}\right] \quad (1)$$

where σ_{HB} is equal to the diameter of DC*X* beads (0.2*d*). The potential is smoothly shifted to zero and cut off in the region of $1.9\sigma_{HB}$ to $2.0\sigma_{HB}$; we note that this LJ potential only varies with *r* and not angles. Despite LJ potential being an isotropic potential, through the choice of bead sizes and placements, these "active" small DC*X* beads, mimicking the −OH group placement, attract each other only over a small region in space, effectively becoming directional in contrast to the isotropic interactions between the much larger (other CG) beads in the model.

We model effective hydrophobic interactions between carbon rings in implicit water, with a 12−6 LJ potential between BB beads as in eq 2

$$U_{BB}(r) = 4\epsilon_{BB}\left[\left(\frac{\sigma_{BB}}{r}\right)^{12} - \left(\frac{\sigma_{BB}}{r}\right)^{6}\right] \quad (2)$$

where σ_{BB} is equal to the diameter of BB bead (1*d*).

Similar to our approach in the original work on cellulose,[35] we model interactions between like, unsubstituted DC beads (DC2−DC2, DC3−DC3, DC6−DC6) with a purely repulsive Weeks−Chandler−Andersen (WCA) potential[37] under an increased cutoff distance of $2.3\sigma_{HB}$ (where $\sigma_{HB} = 0.2d$), as shown in eq 3. This serves as an additional "repulsive shell" to prevent the formation of DC*X*−DC*Y*−DC*X* hydrogen bonding "trimers" and retain the specificity of hydrogen bonds.

$$U_{rep}(r) = \begin{cases} 4\epsilon_{WCA}\left[\left(\frac{2.3\sigma_{HB}}{r}\right)^{12} - \left(\frac{2.3\sigma_{HB}}{r}\right)^{6}\right] + \epsilon_{WCA} \text{ if } r < 2^{1/6} \times 2.3\sigma_{HB} \\ 0 \text{ if } r \geq 2^{1/6} \times 2.3\sigma_{HB} \end{cases} \quad (3)$$

All other pairwise interactions, including those involving "silenced" DC*X* beads, are modeled using the WCA potential with the regular cutoff

$$U_{WCA}(r) = \begin{cases} 4\epsilon_{WCA}\left[\left(\frac{\sigma_{ij}}{r}\right)^{12} - \left(\frac{\sigma_{ij}}{r}\right)^{6}\right] + \epsilon_{WCA} \text{ if } r < 2^{1/6} \times \sigma_{WCA} \\ 0 \text{ if } r \geq 2^{1/6} \times \sigma_{WCA} \end{cases} \quad (4)$$

where ϵ_{WCA} is set to 1 kT and σ_{ij} is equal to $(\sigma_i + \sigma_j)/2$, the average of the diameters of the two involved CG beads.

We capture the solvent effect on MC chains implicitly in the CG MD simulations via the choice of values of ϵ_{HB} and ϵ_{BB}, representing

https://doi.org/10.1021/acs.biomac.3c01209
Biomacromolecules 2024, 25, 1682−1695

the relative affinity between MC chains induced by interchain hydrogen bonds (ϵ_{HB}) and hydrophobic effects (ϵ_{BB}) with solvents of different polarity and/or at different temperatures. We do not know which ϵ_{HB} and ϵ_{BB} correspond to which temperature for water as the solvent, and as such, we refrain from making any conclusions about the phase transition boundary or stages of assembly of MC chains in solutions as a function of temperature. Instead, as shown in the Results Section, we focus only on the assembled structures at various pairs of ϵ_{HB} and ϵ_{BB} and understand how chains pack within these assembled structures.

2.1.2. MD Simulation Protocol with the CG Model. Using the CG model described in the previous section, we run Langevin Dynamics simulations in the *NVT* (i.e., constant number of beads *N*, volume of simulation box *V*, and temperature *T*) ensemble using the LAMMPS package.[38] We prepare the initial configurations by placing 100 MC chains of a chain length *N* in an extended, rod-like conformation on a grid in a cubic simulation box of $300d \times 300d \times 300d$. Within 600,000 timesteps and at a time step size of 0.001τ (τ is the reduced unit of time), the simulation box is compressed to a desired packing fraction of the MC monomer bead in the simulation box (0.0014-0.0028). The simulated packing fractions correspond to ∼0.5 − ∼1 MC wt %, respectively; interested readers can look at Supporting Information Section SB for connections between our simulation box size, packing fraction of MC monomer beads, and experimentally relevant units of MC wt %. During the simulation box size reduction, the temperature is maintained at T = 5.92T* with a Langevin thermostat,[39] and the chains are allowed to relax freely from the initial rodlike state within the gradually shrinking box dimensions. T*, our reduced unit of temperature, corresponds to ∼50.5 K based on our choice of reduced unit of energy, ϵ_0 = 0.1 kcal/mol, so, 5.92T* corresponds to approximately room temperature (298 K). These steps above create the initial configuration that is then used for the simulations of assembly with increasing interchain hydrogen bonding favorability (ϵ_{HB}) and strength of the hydrophobic effect (ϵ_{BB}). While in experimental systems, MC chain assembly into fibrils occurs above room temperature, we instead capture the temperature effect "implicitly" by changing the favorability of hydrogen bonding and hydrophobic interactions (ϵ_{HB}, ϵ_{BB}) rather than changing the simulation temperature itself.

To explore different combinations of interchain hydrogen bonding favorability (ϵ_{HB}) and strength of hydrophobic effect (ϵ_{BB}), we utilize an annealing protocol in which we start from low ϵ_{HB} and ϵ_{BB} and gradually increase the strengths of both types of attractions. This annealing protocol avoids kinetically trapped configurations caused by directly simulating the MC chains at the desired higher values of ϵ_{HB} and ϵ_{BB}. Specifically, we start from ϵ_{BB} = 0.1 kcal/mol and increase the interchain hydrogen bonding strength, ϵ_{HB}, from 2.2 to 5.2 kcal/mol, with a step size of 0.1 kcal/mol every $10{,}000\tau$, or 10 million timesteps. We note that any time step larger in size than 0.001τ resulted in unstable simulations.

The annealing protocol described above generates equilibrated configurations at each ϵ_{HB} while efficiently sampling many ϵ_{HB} values. Then, starting from each of the equilibrated configurations, we attain four selected ϵ_{HB} values− 3.7, 4.2, 4.7, and 5.2 kcal/mol. We run another set of simulations where ϵ_{BB} is increased from 0.2 to 0.5 kcal/mol, with a step size of 0.05 kcal/mol every $4{,}000\tau$. In our previous work, these chosen ϵ_{HB} values covered the range of hydrogen bond strengths that drive the configuration of unsubstituted cellulose from dispersed to aggregated.[35] These ϵ_{HB} values are on the same order of the estimated hydrogen bond strength between cellulose chains, ∼4−7 kcal/mol[40] (note that our ϵ_{HB} models the "excess" interchain hydrogen bond strength compared to the chain-water hydrogen bond strength, not the absolute value of interchain hydrogen bond strength). As for our chosen values of ϵ_{BB} and its connection with realistic values, we note a past atomistic, constrained molecular dynamics study[41] which found that the hydrophobic association energy between two glucose facing each other ring-to-ring is ∼1 kcal/mol. In our CG (implicit solvent) MD studies, we find that dispersed MC chains assemble into fibrils at ∼0.4−0.5 kcal/mol. The lower value of our CG MD simulations' ϵ_{BB} in real units as compared to the 1 kcal/mol value seen in atomistic calculations[41] is not surprising as the former (∼0.4−0.5 kcal/mol) is an effective isotropic CG interaction between spherical BB beads and the latter (∼1 kcal/mol) is calculated as the anisotropic effective interaction between two rings facing each other in explicit water. Thus, our selected values of ϵ_{HB} and ϵ_{BB} in the CG MD simulations are realistic.

For analyses, we used the last configuration at each ϵ_{BB} stage. This is because the simulations at high attraction strengths exhibit little variability in structures during equilibration and we cannot sample multiple uncorrelated configurations. So, instead of taking multiple (likely correlated) configurations, we use for analyses only the final configurations at the specific attraction strengths from three independent runs originating from the same initial configurations.

2.1.3. Analyses of CG MD Simulation Trajectories. Using in-house codes, we identify the formation of fibrils and the diameters of the fibrils.

2.1.3.1. Identification of Fibrils. We first divided the simulation box into grid cells. In practice, we have found that a ∼15 × 15 × 15 grid division of the simulation box, resulting in a cell size of $(3-5d)^3$, gives us meaningful results based on our visual observations of the fibril configuration. For each cell, we identify all segments of bonded MC monomers in the cell and calculate the weighted average orientation of all the segments using this equation

$$v_{i,j,k} = \frac{\sum_n L_n v_n}{\sum_n L_n} \tag{5}$$

where L_n is the segment length (number of monomers) of the *n*-th segment in the cell $[i,j,k]$ and v_n is the head-to-tail vector drawn between the center of the first monomer of that segment and the center of the last monomer of that segment. The choice of head (first) and tail (last) of a segment is irrelevant, and the orientation of the vectors is defined to always point to the + *x* direction. This definition avoids the issue of any two vectors that are ∼180° from each other being treated as opposing vectors and canceling each other out in the above calculation.

After $v_{i,j,k}$ is calculated, the orientational order for the cell is calculated as

$$S_2(i,j,k) = \left\langle \frac{3\cos\theta_n - 1}{2} \right\rangle \text{ for all } n \text{ segments in the cell}[i,j,k] \tag{6}$$

where θ_n is the angle between $\boldsymbol{v_n}$ and $\boldsymbol{v_{i,j,k}}$. A cell with many chain segments can have an S_2 value between 0 when the chain segments have random orientations and 1 when all chain segments are orientationally aligned.

After this last calculation on every cell, for every cell, we have an average orientation $\boldsymbol{v_{i,j,k}}$ and an orientational order parameter S_2. Based on these two factors, we then apply a breadth-first search[42] based on the "friend-of-friend" algorithm to connect neighboring cells with significant orientational order and similar average orientation into ordered domains of fibrils. A cell $[i,j,k]$ will be added to an existing fibril domain if it satisfies all of these conditions

(1) The cell is immediately neighboring to another cell that is already in that ordered domain along the *x*, *y*, or *z* directions.
(2) The cell has an S_2 value [i.e., S_2 (i,j,k)] of at least 0.3.
(3) The average orientation of the cell $(v_{i,j,k})$ is no more than 30° different from the orientation vector of any other cell, as can be equivalently described by the following equation:

$$v_{i,j,k} \circ v_{i',j',k'} < \sin(30^\circ) \text{ for } \forall\, [i',j',k'] \text{ already in the ordered domain} \tag{7}$$

We do not use explicit distance-based cutoff criteria to identify aggregated monomers as the contact distance is different depending on whether the aggregation is due to hydrogen bonds or hydrophobic effects, which are represented by potentials with different cutoff values. We instead assign chains in the proximity of a cell to be assembled. In Figure 2, we show two representative simulation boxes with assembled fibrils.

https://doi.org/10.1021/acs.biomac.3c01209
Biomacromolecules 2024, 25, 1682−1695

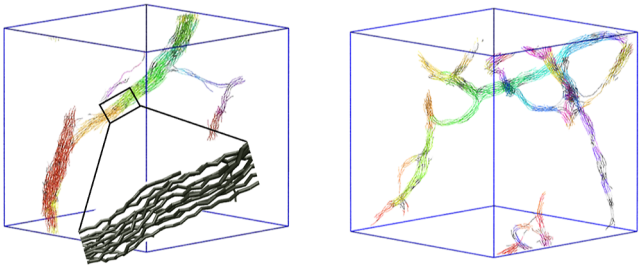

Figure 2. Fibril domains were identified by our in-house algorithm. Fibril domains are represented by (nonblack) colors. The chain segments shown in black belong to isolated cells that cannot be attributed to any fibril domain. The inset of the left panel shows the zoom-in of one of the fibril domains showing only the chain BBs with a matchstick representation; this confirms that individual chains stack in an orientation aligned with the fibril axis.

2.1.3.2. Calculation of Fibril Radius. For each connected fibril domain consisting of monomers from at least 5 different chains, we calculate the geometric center of the domain $[x_c, y_c, z_c]$ by taking the average x, y, and z coordinates of all BB beads in the fibril (after proper wrapping based on periodic boundary conditions). We then calculate the average orientation of the entire fibril domain (ν_f) using the following equation, like eq 5

$$\nu_f = \frac{\sum_n L_n \nu_n}{\sum_n L_n} \tag{8}$$

where n loops through all segments of monomers in the domain. Next, we define a principal axis of the fibril domain as a line parallel to ν_f and going through $[x_c, y_c, z_c]$. We then calculate the distance from all BB beads in the fibril to the principal axis of the fibril domain and take the largest value as the radius of the fibril domain. We report the average fibril diameter (twice the calculated radius) of all fibrillar domains in a simulation snapshot as the final average diameter of the entire configuration. To account for varying contour lengths of fibril domains, the fibril domains are weighed by the total number of MC monomers included in the domain when calculating the average fibril diameter.

2.1.4. Parameter Space Explored Using CG MD Simulation. In the CG MD simulations, we study the structure of the MC assembly for chain lengths (N) of 40 (monomers), 75, 100, and 250. These chain lengths correspond to 7.4 to 47 kg/mol molar masses for MC chains and overlap with the molecular weights considered in previous experimental studies where MC chains as low as 22 kg/mol were studied.[17] We study the above chains at ∼0.5 and ∼1 wt %, which correspond to 0.0014 and 0.0028 packing fraction of monomers (i.e., volume of MC chains' BB beads divided by simulation box volume); as noted earlier in Supporting Information Section SB, we demonstrate how we calculate the corresponding wt % from our simulation box composition. Our choices are inspired by past experimental studies of MC solutions where they focused on concentrations ranging from 0.1 to ∼3 wt %, usually below 1 wt %.[1,14,17,22,43−45] Lastly, as the CG MD simulation study of MC chains focuses on the effect of MC chain length and concentration on fibril assembly, we maintain the methoxy substitution pattern at 0.7 on O2H (DC2), 0.5 on O3H (DC3), and 0.6 on O6H (DC6), similar to known DS of commercial cellulose.[2]

2.2. Atomistic MD Simulations. *2.2.1. Model.* We perform all-atom (AA) MD simulations of MC chains in explicit water using GROningen MAchine for Chemical Simulations (GROMACS) version 2018.1.[46] We use the GROMOS 56A(CARBO) force field,[47] a variation of GROMOS force field optimized for hexopyranose-based carbohydrates. The GROMOS 56A(CARBO) force field reproduces experimentally determined relative free energies of ring conformers, anomers, epimers, hydroxymethyl rotamers, and glycosidic linkage conformers for dilute cellulose systems.[47,48] GROMOS 56A(CARBO) is already parametrized for cellulose but not for MC; to accommodate methyl substitutions, we made some edits to the files in the open-source repository hosting the force field for GROMACS; we direct the reader to Supporting Information Section SC for this information. Hydroxy groups' hydrogens are modeled explicitly, while aliphatic groups' hydrogens are modeled implicitly within united atoms.For water molecules, we use the simple point charge water model[49] because it has been found to be compatible with the GROMOS 53A6 force field,[48] a force field closely related to the GROMOS 56A(CARBO) force field that we use.

The initial configuration that we use in these atomistic simulations is a preassembled fibril of MC chains. This preassembled fibril of MC chains is built using the Cellulose Builder toolkit[51] where we place the desired number of MC chains aligned and parallel to each other with the relative chain placement matching that of cellulose-Iβ crystals (Figure 3).[52] We note that while there are other cellulose polymorphs

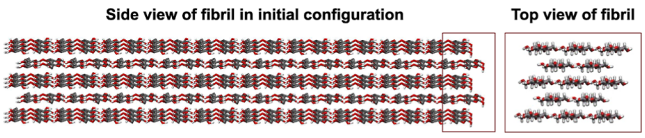

Figure 3. Initial configuration of a MC fibril—side and top views.[50,51] During the energy minimization and equilibration stages, the MC chains deviate from this initial ordered configuration because of repulsion between the methyl groups and water molecules penetrating within the fibril to form hydrogen bonds with the hydroxyl groups.

with antiparallel chain alignment between sheets (i.e., in the opposite head-to-tail direction),[53] we choose our initial configuration based on the parallel configuration of cellulose-Iβ crystals. Our choice of the initial configuration is justified partly by CG MD simulation results (see, for example, Figure 2 or the detailed results discussed later) where MC chains are aligned with the fibril axis within the assembled MC fibrils. At the same time, we choose an initial configuration for the MC chains without any twists to objectively test if AA simulations also show MC chain twisting.

We place the atomistic MC chains in the preassembled state in the center of each simulation box with a buffering distance of 3.0 nm between the outermost MC monomers in the fibril and the edge of the box. The explicit water molecules are randomly inserted in all vacant spaces of the box. The simulation box size is chosen to be sufficiently large to accommodate the MC fibril without self-interactions via periodic boundary conditions. We determine the size of the simulation box separately for each system (i.e., depending on the number and length of MC chains), with details about box dimensions recorded in Supporting Information Table S4.

2.2.2. AA MD Simulation Protocol. The initial configurations of the MC chains and water molecules are subjected to an initial energy minimization step using the steepest descent minimization algorithm.[54] During this energy minimization step, short-range electrostatics and van der Waals interactions are cut off at 1.0 nm, and long-range electrostatics are included using the particle mesh Ewald method.[55] Following the energy minimization, we run the system in the *NVT* ensemble (constant number of particles, volume, and temperature) for 1 ns to ensure that we achieve stabilization at the desired temperatures, either 300 or 348 K. These temperatures are chosen so that we can determine differences in the structure and effective interactions with MC chains at temperatures below and above the MC gelation temperature of ∼323 K in water. We use the velocity-rescaling thermostat for this step because it produces the correct canonical ensemble while still having the advantages of first-order decay of temperature deviations.[46,54] All bonds involving hydrogens in MC chains are restrained in this NVT step using the LINCS holonomic constraint algorithm.[56]

After confirmation of the desired temperature has been achieved in the *NVT* ensemble, an isothermal−isobaric (*NPT*) simulation is performed for 40 ns. We maintain a constant pressure of 1.0 bar using the Parrinello−Rahman coupling barostat[57] and maintain the temperature constant at 300 or 348 K using the Nosé−Hoover

https://doi.org/10.1021/acs.biomac.3c01209
Biomacromolecules 2024, 25, 1682−1695

thermostat.[58] Equilibration in the *NPT* ensemble stabilizes the pressure and the density of the system prior to data collection. We ensure that the structures of MC chains and water have equilibrated by monitoring the analysis metrics in Section 2.2.3, confirming that they have stopped evolving and fluctuate around a consistent value by the end of simulation. In all cases, we conducted analyses using the last configurations sampled from five independent simulation runs of each system.

2.2.3. Analyses on AA MD Simulation Trajectories. We first preprocess all AA simulation trajectories with the following two steps for consistency and to facilitate calculations described below: (1) shifting the periodic boundaries so that the fibrils are centered in the box. This step ensures that none of the chains are cut by the edges of the simulation box; (2) adding a "center of monomer (COM)" pseudobead for each monomer in each snapshot by taking the average positions of the five carbon atoms (C1, C2, C3, C4, C5) and one oxygen atom (O5) on the anhydroglucose ring. The COM pseudobeads are used repeatedly in calculations described below to represent the position of the entire monomer.

2.2.3.1. End-to-End Chain Distance Calculation. To quantify the extent of twisting of MC chains, we calculate the end-to-end distance of the chain (R_{ee}) as the distance between the COM pseudobeads of the first and last monomer of each chain. We also define the R_{ee} of the entire fibril segment as the average R_{ee} of all of its chains.

2.2.3.2. Constructing a Voronoi Diagram. Given the position of MC monomers (represented by the coordinate of COM pseudobeads) and water molecules (represented by the coordinate of the oxygen atoms), we use Voronoi tessellation[59] to partition the space within the simulation box into regions that each enclose one and only one MC monomer or water molecule. The partitioned Voronoi region containing the MC monomer or water molecule is then treated as the volume "occupied" by that monomer or water molecule. From the Voronoi tessellation, we derive a set of results we report in the Results section (Section 3.2), including the number of water neighbors, the number of "dry monomers", and the total volume of the fibril. More details of these analyses can be found in the Supporting Information (Section SD). We carry out all Voronoi tessellation-related calculation using Scipy,[60] specifically the *scipy.spatial.voronoi* class (for the tessellation) and the *scipy.spatial.ConvexHull* class (for calculating the volume of the partitioned Voronoi regions).

2.2.3.3. Twisting of a Local Segment of the Chain. To probe the relationship between the twisting of an MC chain segment and the local density of methyl groups surrounding the segment, we also define a metric called "deviation angle" to quantify the extent of twisting of a segment of chains with respect to the overall fibril orientation. We discuss the definition and nuances of this metric in the Results section (Section 3.2) and corresponding figure in Supporting Information (Figure S5), within the context of other results that motivate us to calculate this metric.

2.2.4. Parameters Varied in the AA MD Simulation. We vary the number of chains (13, 25), degree of polymerization (DP)(20 mers, 30 mers), and DS [DS = 0 (cellulose), 0.6, 1.2, 1.8, 2.4, 3 (fully substituted MC)] of the MC chains in a fibril. To achieve the intermediate DS values between 0 and 3, we randomly replaced some of the −OH groups with $-OCH_3$ groups (where C-H is implicit, within united atoms) at positions 2, 3, and 6 using an in-house Python code.

We choose 13 and 25 chains to evaluate whether results change with an increased number of chains while maintaining the same Iβ crystal packing structure as detailed previously. Iβ cellulose crystals pack in a manner that is staggered. In the 13-chain configuration, there are five stacks of MC sheets that alternate between 2 and 3 monomers in width (Figure 3). In this manner, there is effective sampling of both internal chains (surrounded only by other MC chains) and external chains (exposed to water). The amount of 25 chains is selected to evaluate the effect of the number of chains in the fibril while maintaining the Iβ crystal packing. In the 25-chain configuration, there are seven stacks of MC sheets that alternate between 3 and 4 monomers in width. In this manner, we also have more sampling of internal chains (surrounded by other MC chains and potentially not in direct contact with water).

We choose 20 and 30 repeat units (20-mers and 30-mers) to establish the effect (or the lack thereof) of the DP (chain length) on the trends in our results. 20-mers are selected to have a sufficiently long chain to visualize large-scale structural changes. We select 30-mers, a 50% increase in monomers-per-chain to determine how such an increase in chain length affects the effective entropic and enthalpic interactions contributing to fibrillation and the water contacts inside the fibril.

The two temperatures chosen—300 and 348 K—are above and below the gelation temperature of commercial MC with DS = 1.8, ~323 K.[1] For each set of fibril dimensions, temperature, and DS, 5 independent trials are performed to quantify the variance of fibrillar structures and water penetration between trials and ensure that the simulations do not demonstrate kinetic trapping.

3. RESULTS

3.1. Assembly of MC Chains into Fibrils. We present in Figure 4 the representative structures observed at the last time step of simulations at various values of hydrogen bonding strength (ϵ_{HB}) and hydrophobic effect strength (ϵ_{BB}); these structures are all at the same molecular weight (100-mer) and wt % of MC. As noted earlier, we want to identify chain packing within assembled states at various values of these interaction strengths because at the realistic temperatures in experiments, the MC chains likely experience both of the driving forces to different extents. We find that the hydrogen bonding effect and hydrophobic effect both promote MC chain assembly, with the MC chains forming fibrils as ϵ_{HB} is increased or as ϵ_{BB} is increased. At sufficiently high ϵ_{HB} and/or ϵ_{BB}, virtually all MC chains become part of the fibril structure. The top right inset in Figure 4 shows that the chains pack in an aligned configuration within the fibril. This type of chain packing is in agreement with the latest experimental evidence that the fibril contour length increases with chain molecular weight[17] and WAXS measurement about the correlation between chain orientation and fibril orientations.[22] We also do not observe meaningfully consistent formation of toroidal structures at any point during the simulation as assumed in some previous CG MD simulations.[25,26,28,29]

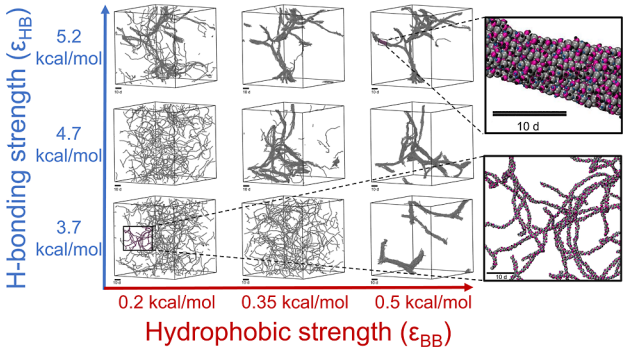

Figure 4. Representative simulation snapshots of 100-mer MC chains at ~1 wt % at different hydrogen bonding strengths (ϵ_{HB}) and hydrophobic effect strengths (ϵ_{BB}). The black bars in the bottom left corners of the snapshots correspond to 10d (d is the reduced unit of length). These configurations are saved at the end of each stage where ϵ_{BB} is kept constant, and these images are rendered using Visual Molecular Dynamics (VMD).[50] The reader is directed to the method section, where we discuss realistic scenarios where such hydrogen bonding and hydrophobic effect strengths would be seen.

https://doi.org/10.1021/acs.biomac.3c01209
Biomacromolecules 2024, 25, 1682−1695

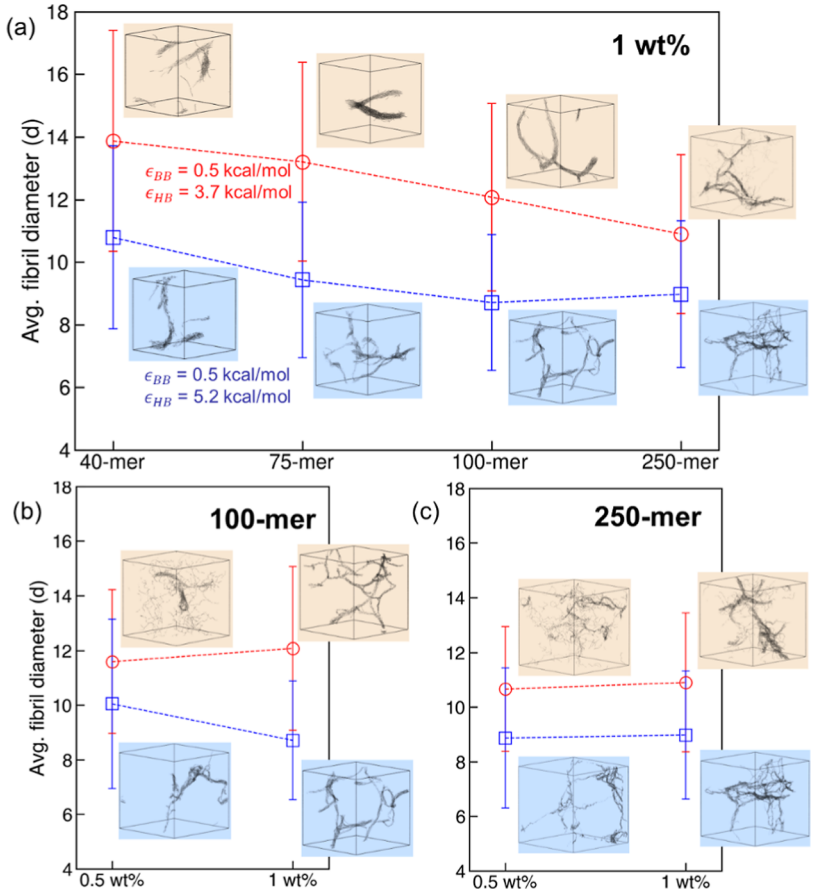

Figure 5. Average fibril diameter of MC chains (a) at ∼1 wt % of different chain length as noted in the *x*-axis and (b,c) of 100-mers and 250-mers, respectively, at different weight percentages as noted in the *x*-axis. Red curves represent assembly at ϵ_{HB} = 3.7 kcal/mol, ϵ_{BB} = 0.5 kcal/mol and blue curves represent assembly at ϵ_{HB} = 5.2 kcal/mol, ϵ_{BB} = 0.5 kcal/mol. Error bars indicate the standard deviation between diameters of different fibril segments across all three trials. Simulation images are set to a similar size for visual clarity even though the actual simulation box sizes scale with chain lengths and weight percentages.

While MC chains always form fibrils, there are some noticeable differences in the structure of the fibrils depending on the type of interaction and its strength. Fibrils formed when the hydrophobic effect dominates (e.g., at ϵ_{BB} = 0.5 kcal/mol, ϵ_{HB} = 3.7 kcal/mol) are larger in diameter and less bifurcated than the fibrils formed when the hydrogen bonding effect dominates (e.g., at ϵ_{BB} = 0.5 kcal/mol, ϵ_{HB} = 5.2 kcal/mol). In Figure 5, we quantify such a difference with the calculated average diameters of MC fibrils at varying MW and weight percentage at ϵ_{BB} = 0.5 kcal/mol, ϵ_{HB} = 3.7 kcal/mol, and ϵ_{BB} = 0.5 kcal/mol, ϵ_{HB} = 5.2 kcal/mol. We find that indeed, a stronger hydrogen-bonding effect leads to a significantly lower fibril diameter. To explain this difference in fibril diameters for the two driving forces—H-bonding and hydrophobicity—let us assume that the fibril diameter is controlled by the balance between the interchain attraction (favoring fibril growth) and entropic penalty for chains to assemble and align (hindering fibril growth). With this assumption, we can explain this difference in fibril diameter between the two driving forces in this manner: There must be a heavier entropic penalty for chains to assemble via directional hydrogen bonds specifically between aligned −OH groups (DCX beads in our model) than the entropic penalty for chains to assemble via isotropic hydrophobic attraction between rings in the monomers (or BB beads in our model). This difference between the two driving forces is further exaggerated by the scarce hydrogen bonding capabilities of MC compared with unsubstituted cellulose.

Most notably, at the same values of ϵ_{BB} and ϵ_{HB}, fibrils formed at the different chain lengths and MC concentrations all have similar average diameters of ∼12−14*d* at ϵ_{BB} = 0.5 kcal/mol, ϵ_{HB} = 3.7 kcal/mol and ∼8−10*d* at ϵ_{BB} = 0.5 kcal/mol, ϵ_{HB} = 5.2 kcal/mol. This consistency in fibril diameters agrees with results from analysis of small-angle scattering measurements[17,23] that found an average diameter of 17−20 nm for varying MC chain length and weight percentage in solution. The similarity in fibril structures at the same interaction strengths can also be visually observed from the simulation snapshots accompanying Figure 5. However, we do not expect that the average fibril diameters will always remain consistent at a higher MC concentration. In Supporting Information Figure S2, we examine the MC assembly of 100-mers at ∼4 wt %, which is higher than the wt % considered in past experiments (usually ≤3 wt %).[1,14,17,22,43−45] The simulation configurations are shown in Figure S2a at ϵ_{HB} = 3.7 kcal/mol, ϵ_{BB} = 0.5 kcal/mol shows assembled fibrils of larger diameters than the fibrils found at ≤1 wt % (Figure 5). We also see three-dimensional aggregates coexisting with 1D fibrils, serving as "crosslinking areas" between multiple 1D fibrils; while this is confirmed visually, we note that our fibril identification algorithms tend to be inaccurate in extracting 1D fibril regimes when there are prevalent 3D aggregates at the

https://doi.org/10.1021/acs.biomac.3c01209
Biomacromolecules 2024, 25, 1682−1695

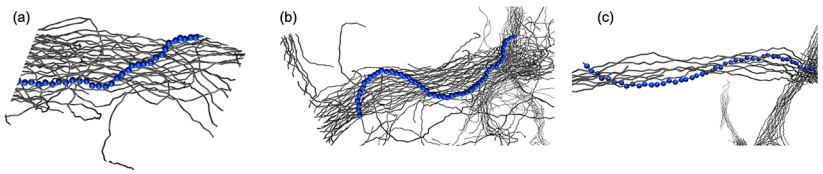

Figure 6. Representative simulation snapshots of a fibril highlighting a segment of one MC chain that has adopted a twisted configuration (shown in blue). Snapshots are taken from simulations of (a) 250-mers at ∼1 wt %, ϵ_{HB} = 3.7 kcal/mol, ϵ_{BB} = 0.5 kcal/mol, (b) 100-mers at ∼1 wt %, ϵ_{HB} = 3.7 kcal/mol, ϵ_{BB} = 0.5 kcal/mol, and (c) 100-mers at ∼1 wt %, ϵ_{HB} = 4.7 kcal/mol, ϵ_{BB} = 0.5 kcal/mol.

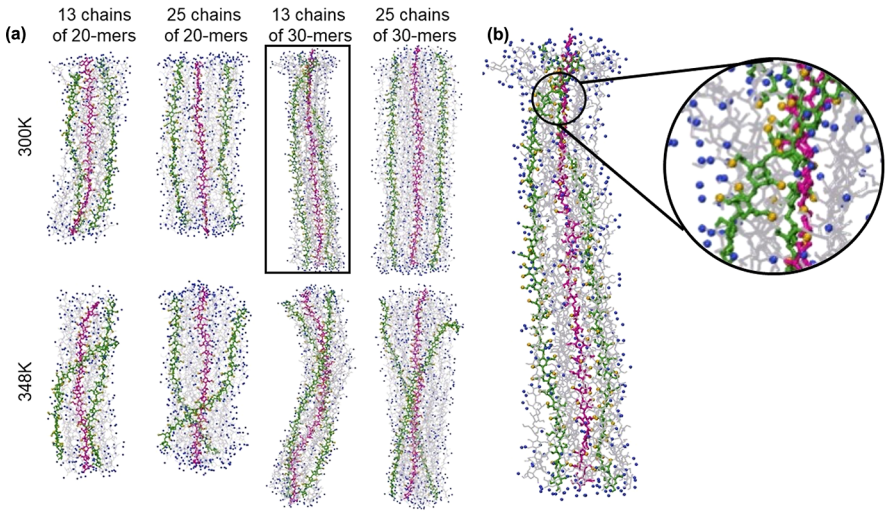

Figure 7. Representative simulation snapshots of the final configurations of commercial MC fibrils (DS = 1.8) in the atomistic simulations. Two chains that exhibit twisting near the surface of the fibril are colored green; one chain with less twisting near the center of the fibril is highlighted in magenta. Methoxy groups from the selected chains are highlighted in yellow and water contacts (water within 0.6 nm of the fibril) are shown as blue spheres. (b) Zoom-in view of 13 30-mers at 300 K in (a), highlighted in the black rectangle.

intersection of fibrils. We also see instances of fibrillar segments "merging" into aggregates of a larger length scale (two examples shown in Figure S2b). These results suggest that at a sufficiently high MC concentration, fibrils can behave differently from the dilute regime and potentially form higher length scale hierarchical assemblies. We note that at ϵ_{HB} = 5.2 kcal/mol, ϵ_{BB} = 0.5 kcal/mol, we do not see an assembly configuration at ∼4 wt % as different from lower wt % as at ϵ_{HB} = 3.7 kcal/mol, ϵ_{BB} = 0.5 kcal/mol; this suggests that the "critical" MC weight percentage at which the assembly behavior deviates from the dilute regime can also be a function of the interaction strengths or temperature.

We report our fibril diameters in reduced units of length (1*d*). We cannot convert these numbers to real units because our MC CG model is extended from the cellulose MC model where 1*d* corresponds to the size of the cellulose monomer in the crystalline state (∼0.5 nm); this is not expected to be the size of a more hydrated MC monomer in implicit water. One must compare dimensions of the solvated MC monomer to the relatively dehydrated cellulose monomer in crystals in a rigorous manner to map the values of MC fibril diameters seen in the CG simulation to real units (nm). We expect that MC fibrils will contain more amounts of water than cellulose crystals,[17,61] and this solvated monomer size has to be considerably larger than a relatively dehydrated cellulose monomer in a crystal. In addition to the unknown monomer size, we are also not able to map the thermodynamic conditions corresponding to the fibrillation temperature for MC in water to our ϵ_{HB} and ϵ_{BB} values without further rigorous potential mean force calculations. As the focus of this paper was to understand how chains assemble into fibrils, we are content with the agreement between our simulations and experiments of observing consistent fibril diameter for varying chain length and concentrations (≲1 wt %). For a future publication, where we will conduct CG MD simulations of MC chains' assembly for varying degrees of methoxy substitution (DS), we will delve into the necessary computations needed to calculate the solvated MC monomer size and strength of thermodynamic driving forces in real units as a function of DS.

Next, we discuss further the twisted MC chain conformations that we see within these fibrils. As shown in a representative image in Figure 6, some MC chains adopt a twisted conformation, especially in the cases where hydrophobic effect dominates. To the best of our knowledge, while some previous studies have alluded to the MC chain twisting[3,17,22,62,63] (with indirect evidence from modulation in intensity along the fibril in microscopy images[62] or preferred absorption of right-handed light in circular dichroism[63]), no one has conclusively shown twisting with measurements at chain level resolution. However, such twisting has been incorporated in the recent models of chain stacking in alignment with the fibril axis for the internal structure of MC[17] and observed in atomistic simulations of the unsubstituted cellulose nanocrystal.[64−66] Previous computational studies on generic self-attractive semiflexible polymers forming bundles of finite diameters have also found some twisted chains in the bundles.[32−34] To confirm if this chain twisting we see in our CG MD simulations of MC chains in implicit water is also seen with MC chains and explicit water, we use atomistic simulations where the MC chains are initially

https://doi.org/10.1021/acs.biomac.3c01209
Biomacromolecules 2024, 25, 1682−1695

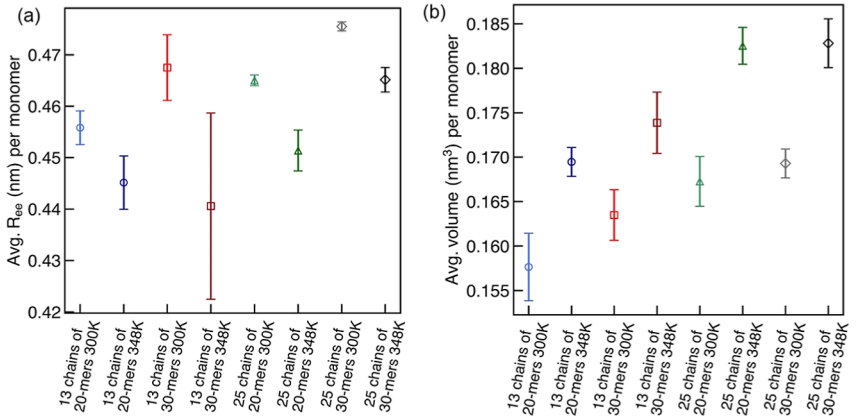

Figure 8. (a) Average end-to-end chain distance (nm) for commercial MC (DS = 1.8) normalized by the number of monomers in each chain and (b) average Voronoi volume per monomer for commercial MC (DS = 1.8) at 300 and 348 K. Error bars for both plots represent standard deviation between the last configuration from 5 independent trials.

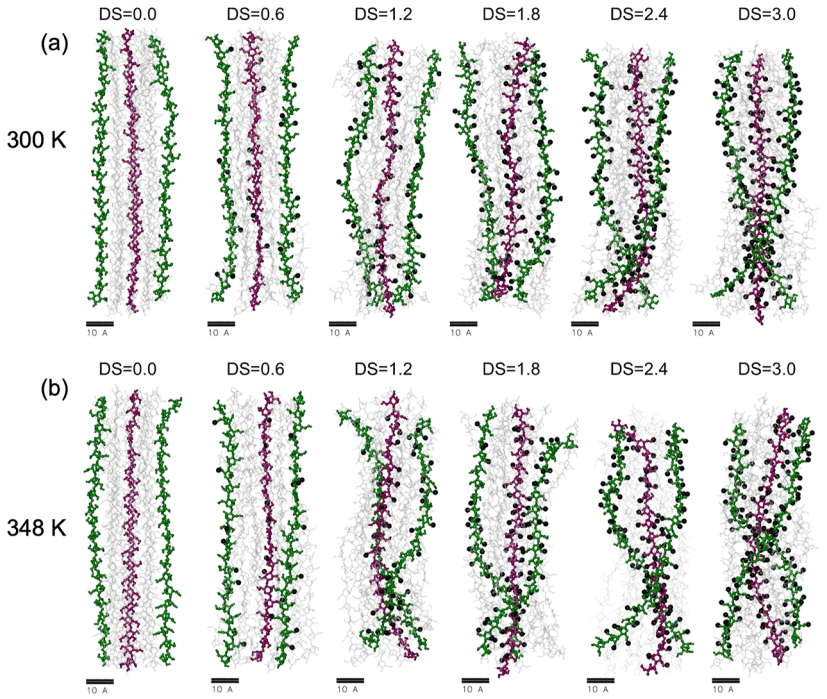

Figure 9. Representative simulation snapshots of the final configurations of systems of 13-chains of 20-mers at increasing DS at (a) 300 and (b) 348 K. Snapshots are rendered using Visual Molecular Dynamics.[50] Two chains that exhibit twisting near the surface of the fibril are highlighted in green; one chain with less twisting near the center of the fibril is highlighted in magenta. Methoxy groups from the selected chains are highlighted in black.

in a preassembled fibril (without any chain twists) and surrounded by explicit water molecules. Through these atomistic simulations of MC chains in explicit water, we confirm that some of the MC chains in the fibrils twist and then probe the molecular underpinnings of such twisted chain conformations.

3.2. Molecular Packing within the MC Fibrils. In Figure 7, we show the representative snapshots of MC chains with commercial DS = 1.8 obtained from atomistic simulations of MC chains in explicit water; these are the final configurations from one of the simulation runs for each of the eight systems with different chain lengths (20-mer and 30-mer) and number of chains (13 and 25 chains) in the fibril at T = 300 and 348 K. As highlighted in Figure 7, we see consistently that some MC chains in the fibril adopt twisted conformations along their backbones; we only highlight three chains for each system for easier visualization of any two chains in twisted conformations against one minimally twisted chain. We also observe that in many cases, the twists are seen in certain portions of the MC chains; at each temperature (300 or 348 K) we observe similar twisting or portions of twisted chains for different chain lengths (20-mer vs. 30-mer) or number of chains (13-chains vs. 25-chains). However, when comparing different temperatures for the same system, some of the chains in the fibrils, especially the chains that are on the external surface of fibril, exhibit a more pronounced twisted conformation at 348 K than at 300 K.

We quantify chain-level and monomer-level information that could explain the fibril-level observation described above. We first calculate the average end-to-end chain length (R_{ee}) for the MC chains inside each fibril, in Figure 8a. The end-to-end

https://doi.org/10.1021/acs.biomac.3c01209
Biomacromolecules 2024, 25, 1682−1695

chain length is calculated as the average distance between one terminal end of the polymer chain and the other terminal end of the polymer chain. We further normalize the results by DP to fairly compare the chain twisting between the two chain lengths (20-mer and 30-mer) we study. The normalized R_{ee} values at 348 K are smaller than at 300 K in all cases, suggesting that some MC chains have transitioned from an extended chain configuration to a partially/fully twisted configuration.

Next, at the monomer-level, we calculate the average Voronoi volume for each monomer[67] and find that this value, a measure of the sum of van der Waals volume occupied by the atoms in each monomer and the free volume around each monomer, is consistently greater at 348 K compared to at 300 K at different chain lengths and/or number of chains (Figure 8b). Correspondingly, we see in Supporting Information Figure S3 that there are fewer number of water contacts for each monomer at 348 K as compared to 300 K. As the van der Waals volumes of the atoms in the monomer do not change between different temperatures, these two sets of results together show that water molecules vacate the volume around the MC monomers at 348 K likely because of hydrophobicity effects dominating at a higher temperature. By water vacating the volume around each monomer, there is more free volume around each MC monomer.

So far, based on the results presented, we conclude that for commercial MC chains (DS = 1.8) as the hydrophobic effect becomes more prominent at elevated temperatures, MC chains in the fibrils twist and adopt a compact spatial arrangement, making the methylated monomers less solvated by water molecules. One could envision the chain twisting in a fibril and simultaneous reduction in monomer-water contacts to be like the relatable act of "wringing out a wet towel" to release water.

3.3. Effect of Extent of Methylation (DS) on MC Chains' Hydration. The atomistic results presented above for commercial MC (DS = 1.8) reveal phenomenologically the structural changes of MC at elevated temperatures due to the dominant hydrophobic effect originating from the added methyl groups. To directly connect the degree of methylation and extent of structural change, next we discuss results from atomistic simulations of MC chains at other DS and investigate the difference in MC fibril structures at various values of DS.

Moving beyond the commercial MC (DS = 1.8), we investigate effects of varying DS from 0.0 to 3.0, where 0.0 is unmodified cellulose and 3.0 is fully methylated MC. In Figure 9, we present representative images of the MC fibrils highlighting a few chains—two green chains that exhibit some twisted conformations and, to contrast, one magenta chain with relatively nontwisted conformation. We find that the twisting of chains is more significant at 348 K compared to 300 K, as seen for the commercial MC chains. We see that the occurrence of twisted conformations increases with increasing DS. In the case of DS = 0 (i.e., unsubstituted cellulose), the chains maintain conformations like those in the initial configurations and exhibit minimal to no twisting. As we increase the DS, parts of some MC chains in the fibril, especially those on the exterior sections of the fibril exposed to water, start to adopt a twisted configuration, wrapping around the unexposed chains near the core of the fibril. At DS = 3.0, the twisting is the most prominent among all DS systems studied. We note that even at DS = 3.0, we can still identify internal chains that are considerably less twisted than the external chains, rather than all the chains adopting similarly twisted configurations. For those higher DS chains that do adopt a twisted configuration, the twisting seems consistent all along the chain, without the apparent variation in twisting in different portions of the chain, as observed at low DS. The R_{ee} results (Figure S4) also quantitatively prove that the average chain end-to-end distance decreases as the twisting of fibrils increases.

Our initial hypothesis was that the twists in the external chains had to be restricted to or near the regions of methylation because the associated increasing hydrophobicity in that local segment of the chain and exposure to water must cause the segment to twist to shield the methyl groups. Alternately, one could argue that the twist in the external chains is not localized to a higher density of methyl groups and instead a global (chain-level and fibril-level) response of the external MC chains with methyl groups due to increased overall hydrophobicity. To investigate these scenarios in a bit more depth, we first quantify twists in the chains and see if there is a correlation between the local chain twist and local density of methyl groups.

To quantify twisting of a segment of a chain consisting of X consecutive monomers, we define deviation angle α as the angle between average end-to-end orientation vector of all chains in the fibril and end-to-end orientation vector of the segment, with larger α representing a more twisted segment. Figure S5a presents a schematic for the definition of the deviation angle α. Because cellulose and MC chains natively adopt a tortuous contour, at $X = 2$ (minimum length of the segment), this deviation angle is nonzero even without any twisting. The deviation angle can thus be treated as the sum of native tortuosity of the chain segment and the degree of twisting the chain adopts, with the contribution of native tortuosity diminishing with increasing X, number of monomers in the segment. In Figure S5b, we show the dependence of the average α on the choice of value of X for fibrils consisting of 13 20-mers at DS = 0, 1.2, and 3. As expected, the average deviation angle increases with increasing DS. Specifically at DS = 0, the average deviation angle of all chain segments initially decreases with X and plateaus at $X \approx 5$; we thus fix the value of X to 5 in our following calculations because it represents a segment that is long enough to minimize the effect from native chain tortuosity but not so long that we are no longer investigating the *local* twisting of a chain segment. In Figure S5c, we present on the fibril level the average deviation angle of 5-monomer segments at varying DS for fibrils of 13 20-mers and 25 30-mers. The results in Figure S5c lead to the same conclusion as from the R_{ee} calculations in Figure S4—higher DS leads to increased twisting of the fibril (higher average deviation angle α), confirming the robustness of this deviation angle metric.

Upon validation of this α metric as a reliable method to quantify twisting, in Figure S6, we "zoom into" the individual segments and plot the deviation angle α of each segment of 5 monomers against the total number of methyl groups in the segment (Figure S6a) and total number of methyl groups in the vicinity of the segment, defined as all methyl groups within 0.6 nm of at least one COM pseudoatom in the segment, regardless of whether the methyl group itself is part of the segment (Figure S6b). We hereby limit our calculations to the intermediate DS (1.2 and 1.8) as there are ample statistical representations of monomers with all possible DS in those cases. Contrary to our original hypothesis that local density of methyl groups drives twisting in that section of the chain, we

https://doi.org/10.1021/acs.biomac.3c01209
Biomacromolecules 2024, 25, 1682−1695

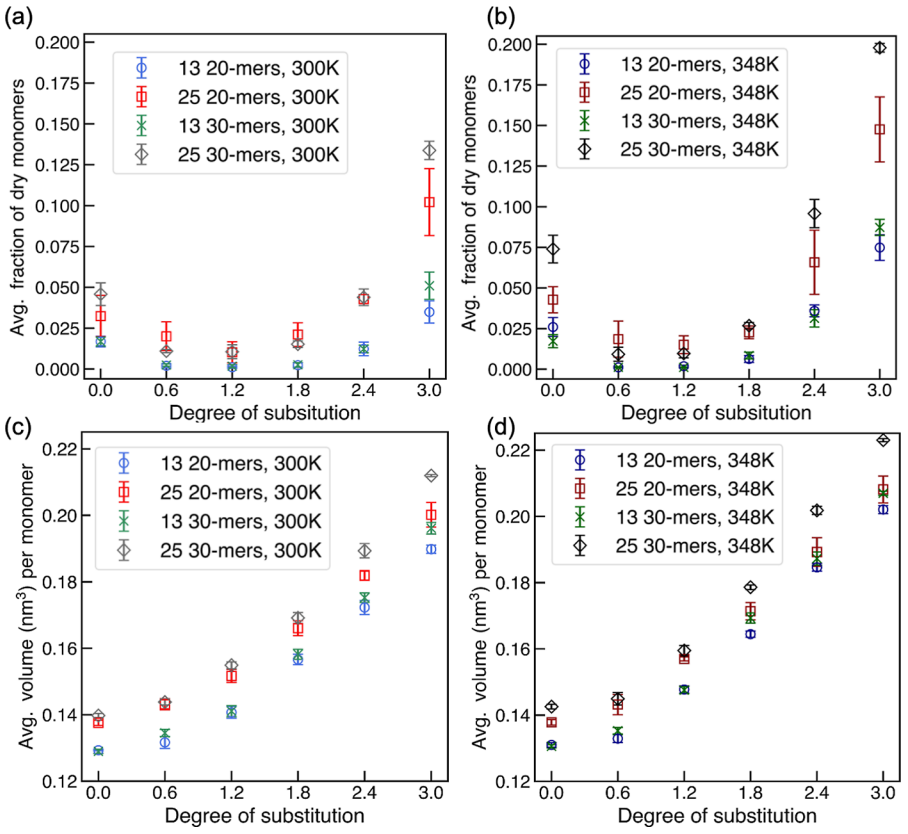

Figure 10. (a,b) Fraction of "dry monomers" and (c,d) average Voronoi volume of fibrils at different DS at (a,c) 300 K and (b,d) 348 K. Error bars represent standard deviation between the corresponding calculations for the last configurations from 5 independent 40 ns trials.

observe no correlation between the extent of methylation of the segment and the extent of twisting for a 5-monomer segment in Figure S6a, with the Pearson correlation coefficient (R) being negligible in all four cases of different chain lengths and number of chains. In Figure S6b, we even notice a weak, negative correlation between the degree of twisting and number of methyl groups in the vicinity of the fibril, although that could be explained by the fact that chain segments near the surface of the fibril tend to be more twisted and coincidentally surrounded by less MC monomers and more water molecules.

Altogether, at an intermediate DS, more methylated chain segments are not necessarily more twisted; we currently do not have a definitive answer to the exact mechanism of how higher methylation globally leads to more twisted fibrils. The twist may be attributed to how the chain manages the increased elastic penalty on the entire chain adopting different configurations to shield methyl groups from water and increased bulkiness of methyl groups vs the hydroxy groups, as a result of (1) the loss of interchain orientational/positional order and (2) the interchain shear and stretch[68] due to deviation from perfectly parallel chain packing.

To understand the hydrophobic effect of methylation on MC chain arrangements in the fibril, we quantify the dry and wet monomers at different DS. In Figure 10a,b, we show the fraction of "dry monomers" defined as MC monomers without any water molecules as Voronoi neighbors, at different DS and both 300 and 348 K. As DS increases from 0 to 3, the number of dry monomers at both temperatures takes a nonmonotonic trend, decreasing from DS = 0 to DS = 1.2 and then increasing until DS = 3.0; this increase is more significant at 348 K than at 300 K. At the higher chain length and/or number of chains, the number of water molecules penetrating the core of the fibril is small, resulting in a large fraction of MC monomers being completely shielded from water contact at high DS, leading to the more significant increase in number of "dry monomers". In Supporting Information Figure S7, we show the average number of water contacts per monomer. Analogous to the trend in the number of "dry monomers", as DS increases from 0 to 3, MC monomer-water contacts decrease until DS ≈ 0.6 or 1.2 and then increase until DS = 3.0; this increase is more drastic at high temperatures. As illustrated in Supporting Information Figure S8, our explanation for this observation is that low to moderate DS (DS > 0 and DS < 1.2) disrupts the hydrogen bonding network of unsubstituted cellulose and allows water to interact with −OH groups that are not hydrogen bonded, thus promoting MC-water interactions. At a higher DS (DS > 1.2), due to presence of methyl groups, there are fewer MC-water hydrogen bonds, and hydrophobicity dominates. This, in turn, drives the MC chains to rearrange and wrap around the core of the fibril to decrease water exposure to the monomers. This nonmonotonicity in water-monomer contacts is also analogous to MC's solubility in water—insoluble as cellulose and soluble at intermediate DS but insoluble again at high DS (and instead soluble in organic solvents).[2]

In Figure 10c,d, we look at the change in Voronoi volume of MC monomers at different DS. As DS increases, the average Voronoi volume of MC monomers always monotonically increases, more significantly so at 348 K than at 300 K. Reasons for this increase could be (1) hydrophobicity driven, i.e., water molecules are driven away from the inside/vicinity of

https://doi.org/10.1021/acs.biomac.3c01209
Biomacromolecules 2024, 25, 1682−1695

fibrils, causing more vacant volumes to be assigned to the fibrils; (2) sterically driven, i.e., the distance between MC chains in the fibrils natively increases because of disruption of the original hydrogen-bonded structure and addition of bulky groups ($-CH_3$). From DS = 0 to ∼1.2, the water-MC contact increases, so the increase in total volume in this regime should be mainly attributed to reason (2)—the inherent swelling of monomer sizes accompanying the frustration of the original crystalline structure stabilized by hydrogen bonds. At DS = 2.4 and 3.0, water is indeed depleted from MC (as shown in Figure 10a,b), so it is possible that both hydrophobic and steric driving forces contribute to the apparent increase in the Voronoi volume of monomers. This conclusion is also supported by the fact that even at 300 K when hydrophobicity is not expected to be significant and we notice some twisting, the Voronoi volume of MC monomers still expands significantly (attributed to an inherent increase in interchain distance), yet by a slightly less extent compared to 348 K (additional expansion of volume attributed to chain rearrangement and water expulsion). This increase in interchain distance also qualitatively agrees with Schmidt et al.[22]'s proposed unit cell of MC crystalline structure that has dimension a (1.14 nm) much larger than that of, e.g., unsubstituted cellulose 1β (a = 0.78 nm, with two chains in the unit cell).[52]

4. CONCLUSIONS

Using a combination of CG and atomistic molecular dynamics simulations, we have systematically investigated the structure of MC chains' assembly into fibrils in aqueous solutions and the molecular packing within the assembled fibrils. We use a CG model for MC chains extended from a previous CG model developed for cellulose that captures the monomer-level variation in the degree and positions of methylation in the MC chains. Using this CG model in MD simulations, we have captured the self-assembly of free, dispersed MC chains into fibrillar structures. Our CG MD simulations have reproduced the experimental observation of consistent average fibril diameter for solutions of MC with varying MC weight percentage (∼0.5 − ∼1 wt %) and molecular weight (40-mers to 250-mers). These CG MD simulations also demonstrate that individual MC chains pack into fibrils with the chains aligning along the long axis of the fibril; these CG MD simulation results have provided critical evidence to resolve a long-standing debate about how MC chains pack in MC fibrils with a finite and consistent diameter of the fibril regardless of chain length and/or solution concentration (0.1−1 wt %).

Besides the insight it provides to understanding MC fibrillar structure, the CG MD simulations' determination of parallel packing of chains is also significant in that it informs us of the initial configuration we should adopt for atomistic simulations. Our atomistic simulations starting from parallel configurations of chains showed how different degrees of methylation and related change in chain hydrogen bonding capability/hydrophobicity have a complex and nonmonotonic effect on the fibril structures and water arrangement around the fibrils. Low to moderate DS (DS < ∼1.2) promote water-chain interactions by disrupting interchain hydrogen bonds and allowing water-chain hydrogen bonds; higher DS renders the chains hydrophobic and expels water from the proximity of the chains. Besides tuning the hydrophobicity, the methylation also seems to contribute to the swelling of the interchain distance compared to cellulose crystals, possibly because of increased steric repulsion of bulky $-CH_3$ groups and the frustration of the original interchain hydrogen bonding network in cellulose crystals.

We also observed twisting of MC chains either in sections of the chain or in the entire chain depending on DS values. These chains are usually found on the exterior of the fibrils in both the CG and atomistic simulations. Atomistic simulations confirmed that such twisting becomes more prevalent with increasing DS and temperature, directly connecting the methylation and related hydrophobicity and increased steric repulsion to the twisting. While more methylation indeed leads to more twisted fibrils, it is not necessary that the twist is restricted to segments of chains where there is a higher density of methylation.

As to why we see consistent diameters of fibrils among the various (DS = 1.8) MC chain lengths and concentrations considered (in the range of 0.1−1 wt %), some previous studies[69,70] suggest that the twisting of semiflexible constituents in a fibrillar assembly is the reason. These past studies argue that the persistence length of the fibril constituent (which in our case is the MC chain) limits the extent to which the constituent can bend in order to twist and wrap around the fibril contour. However, in both our CG and atomistic simulations, the extent of twisting varies both between MC chains and between different segments of the same MC chain; it thus seems unlikely that the stiffness of the chains and the resulting limitation on the maximum possible extent of twisting are the primary cause of finite and consistent fibril diameters.

We offer an alternate potential explanation for the consistent (DS = 1.8) MC fibril diameter for varying chain lengths and concentrations (0.1−1 wt % range). Supporting Information Figure S9 illustrates this working hypothesis. As the MC chains assemble into the fibril, at some point, the fibrils become stiff enough that the chains' entropy loss (going from a free unassembled state to that of being assembled with other chains in a fibril) can no longer be compensated by the enthalpic gain the chains experience upon assembly. This stops the fibrils from growing beyond a specific diameter. Our explanation is supported by our observation of smaller (yet consistent among chain lengths and 0.5−1 wt % concentrations) fibrillar diameters for H-bonding-driven assembly vs that seen for fibrils assembled because of a dominant hydrophobic interaction. Interchain assembly due to localized directional H-bonding between chains has a higher entropic penalty than isotropic hydrophobic interaction-driven interchain assembly because there are fewer number of ways (lower degeneracy) the chain can assemble via H-bonding between specific sites than through isotropic BB−BB attractions. As a result, the assembly of chains into fibrils stops at smaller fibril diameters for those H-bonding-driven fibrils compared to when the assembly is driven by hydrophobic interactions. In the future, we will try to understand how the extent of methylation (DS) of MC chains affects the fibril assembly. To achieve that, we would need to develop CG models of MC chains at varying DS values and use those models in MD simulations with protocols similar to those in the work presented here to predict fibrillar assembly.

■ ASSOCIATED CONTENT

Supporting Information

The Supporting Information is available free of charge at https://pubs.acs.org/doi/10.1021/acs.biomac.3c01209.

https://doi.org/10.1021/acs.biomac.3c01209
Biomacromolecules 2024, 25, 1682−1695

Additional details about the CG model, atomistic force field and protocol, and analyses; details on conversion between weight percentage and simulation box size in CG simulation; and additional results from atomistic simulations (PDF)

AUTHOR INFORMATION

Corresponding Author

Arthi Jayaraman − *Department of Chemical and Biomolecular Engineering, University of Delaware, Newark, Delaware 19716, United States; Department of Materials Science and Engineering, University of Delaware, Newark, Delaware 19716, United States;* orcid.org/0000-0002-5295-4581; Email: arthij@udel.edu

Authors

Zijie Wu − *Department of Chemical and Biomolecular Engineering, University of Delaware, Newark, Delaware 19716, United States;* orcid.org/0000-0001-6269-0244

Audrey M. Collins − *Department of Chemistry and Biochemistry, University of Delaware, Newark, Delaware 19716, United States*

Complete contact information is available at: https://pubs.acs.org/10.1021/acs.biomac.3c01209

Notes

The authors declare no competing financial interest.

ACKNOWLEDGMENTS

Z.W. and A.J.are grateful for the support from National Science Foundation (NSF) CMMT grant #2105744. A. M. C is grateful for support the National Institute of General Medical Sciences of the National Institutes of Health award #T32-GM133395 through the University of Delaware (UD)CBI program. The content is solely the responsibility of the authors and does not necessarily represent the official views of the National Institutes of Health. The CG simulations were run on Caviness supercomputing cluster at UD. Th AA simulations were run on Bridges-2 at Pittsburgh Supercomputing Center through allocation #MCB100140 from the Advanced Cyberinfrastructure Coordination Ecosystem: Services & Support (ACCESS) program, which is supported by National Science Foundation grants #2138259, #2138286, #2138307, #2137603, and #2138296.

REFERENCES

(1) Coughlin, M. L.; Liberman, L.; Ertem, S. P.; Edmund, J.; Bates, F. S.; Lodge, T. P. Methyl cellulose solutions and gels: fibril formation and gelation properties. *Prog. Polym. Sci.* **2021**, *112*, 101324.

(2) Nasatto, P.; Pignon, F.; Silveira, J.; Duarte, M.; Noseda, M.; Rinaudo, M. Methylcellulose, a Cellulose Derivative with Original Physical Properties and Extended Applications. *Polymers* **2015**, *7* (5), 777−803.

(3) Morozova, S. Methylcellulose fibrils: a mini review. *Polym. Int.* **2020**, *69* (2), 125−130.

(4) Heinze, T.; Seoud, O. A. E.; Koschella, A. *Cellulose Derivatives: Synthesis, Structure and Properties*; Springer, 2018..

(5) Vigouret, M. H. Comportement des méthylcelluloses en relation avec leur strsucture. Ph.D. Theses, Université Joseph Fourier, 1996.

(6) Chatterjee, T.; Nakatani, A. I.; Adden, R.; Brackhagen, M.; Redwine, D.; Shen, H.; Li, Y.; Wilson, T.; Sammler, R. L. Structure and Properties of Aqueous Methylcellulose Gels by Small-Angle Neutron Scattering. *Biomacromolecules* **2012**, *13* (10), 3355−3369.

(7) Haque, A.; Morris, E. R. Thermogelation of Methylcellulose. Part I: Molecular Structures and Processes. *Carbohydr. Polym.* **1993**, *22*, 161−173.

(8) Chevillard, C.; Axelos, M. A. V. Phase separation of aqueous solution of methylcellulose. *Colloid Polym. Sci.* **1997**, *275* (6), 537−545.

(9) Kato, T.; Yokoyama, M.; Takahashi, A. Melting Temperatures of Thermally Reversible Gels IV. Methyl Cellulose-Water Gels. *Colloid Polym. Sci.* **1978**, *256*, 15−21.

(10) Chen, C. H.; Tsai, C. C.; Chen, W. S.; Mi, F. L.; Liang, H. F.; Chen, S. C.; Sung, H. W. Novel Living Cell Sheet Harvest System Composed of Thermoreversible Methylcellulose Hydrogels. *Biomacromolecules* **2006**, *7* (3), 736−743.

(11) Thirumala, S.; Gimble, J. M.; Devireddy, R. V. Methylcellulose based thermally reversible hydrogel system for tissue engineering applications. *Cells* **2013**, *2* (3), 460−475.

(12) McAllister, J. W.; Lott, J. R.; Schmidt, P. W.; Sammler, R. L.; Bates, F. S.; Lodge, T. P. Linear and Nonlinear Rheological Behavior of Fibrillar Methylcellulose Hydrogels. *ACS Macro Lett.* **2015**, *4*, 538−542.

(13) Pakulska, M. M.; Vulic, K.; Tam, R. Y.; Shoichet, M. S. Hybrid Crosslinked Methylcellulose Hydrogel: A Predictable and Tunable Platform for Local Drug Delivery. *Adv. Mater.* **2015**, *27* (34), 5002−5008.

(14) Arvidson, S. A.; Lott, J. R.; McAllister, J. W.; Zhang, J.; Bates, F. S.; Lodge, T. P.; Sammler, R. L.; Li, Y.; Brackhagen, M. Interplay of Phase Separation and Thermoreversible Gelation in Aqueous Methylcellulose Solutions. *Macromolecules* **2013**, *46*, 300−309.

(15) Xu, Y.; Wang, C.; Tam, K. C.; Li, L. Salt-assisted and salt-suppressed sol-gel transitions of methylcellulose in water. *Langmuir* **2004**, *20* (3), 646−652.

(16) Nishinari, K.; Hofmann, K. E.; Moritaka, H.; Kohyama, K.; Nishinari, N. Gel-Sol Transition of Methylcellulose. *Macromol. Chem. Phys.* **1997**, *198*, 1217−1226.

(17) Schmidt, P. W.; Morozova, S.; Owens, P. M.; Adden, R.; Li, Y.; Bates, F. S.; Lodge, T. P. Molecular Weight Dependence of Methylcellulose Fibrillar Networks. *Macromolecules* **2018**, *51* (19), 7767−7775.

(18) Fairclough, J. P. A.; Yu, H.; Kelly, O.; Ryan, A. J.; Sammler, R. L.; Radler, M. Interplay between Gelation and Phase Separation in Aqueous Solutions of Methylcellulose and Hydroxypropylmethylcellulose. *Langmuir* **2012**, *28*, 10551−10557.

(19) Zhang, H.; Xie, Y.; Tang, Y.; Ni, S.; Wang, B.; Chen, Z.; Liu, X. Development and characterization of thermo-sensitive films containing asiaticoside based on polyvinyl alcohol and Methylcellulose. *J. Drug Delivery Sci. Technol.* **2015**, *30*, 133−145.

(20) Wollenweber, C.; Makievski, A. V.; Miller, R.; Daniels, R. Adsorption of hydroxypropyl methylcellulose at the liquid/liquid interface and the effect on emulsion stability. *Colloids Surf., A* **2000**, *172* (1−3), 91−101.

(21) Du, M.; Gao, Y.; Han, G.; Li, L.; Jing, H. Stabilizing effect of methylcellulose on the dispersion of multi-walled carbon nanotubes in cementitious composites. *Nanotechnol. Rev.* **2020**, *9* (1), 93−104.

(22) Schmidt, P. W.; Morozova, S.; Ertem, S. P.; Coughlin, M. L.; Davidovich, I.; Talmon, Y.; Reineke, T. M.; Bates, F. S.; Lodge, T. P. Internal Structure of Methylcellulose Fibrils. *Macromolecules* **2020**, *53* (1), 398−405.

(23) Wu, Z.; Jayaraman, A. Machine Learning-Enhanced Computational Reverse-Engineering Analysis for Scattering Experiments (CREASE) for Analyzing Fibrillar Structures in Polymer Solutions. *Macromolecules* **2022**, *55* (24), 11076−11091.

(24) Gartner, T. E.; Jayaraman, A. Modeling and Simulations of Polymers: A Roadmap. *Macromolecules* **2019**, *52* (3), 755−786.

(25) Ginzburg, V. V.; Sammler, R. L.; Huang, W. J.; Larson, R. G. Anisotropic Self-Assembly and Gelation in Aqueous Methylcellulose-Theory and Modeling. *J. Polym. Sci., Part B: Polym. Phys.* **2016**, *54* (16), 1624−1636.

(26) Huang, W.; Ramesh, R.; Jha, P. K.; Larson, R. G. A Systematic Coarse-Grained Model for Methylcellulose Polymers: Spontaneous

Ring Formation at Elevated Temperature. *Macromolecules* **2016**, *49*, 1490−1503.
(27) Huang, W. J.; Dalal, I. S.; Larson, R. G. Analysis of Solvation and Gelation Behavior of Methylcellulose Using Atomistic Molecular Dynamics Simulations. *J. Phys. Chem. B* **2014**, *118* (48), 13992−14008.
(28) Sethuraman, V.; Dorfman, K. D. Simulating precursor steps for fibril formation in methylcellulose solutions. *Phys. Rev. Mater.* **2019**, *3* (5), 055601.
(29) Li, X.; Bates, F. S.; Dorfman, K. D. Rapid conformational fluctuations in a model of methylcellulose. *Phys. Rev. Mater.* **2017**, *1* (2), 025604.
(30) Schmid, F. Understanding and Modeling Polymers: The Challenge of Multiple Scales. *ACS Polym. Au* **2023**, *3* (1), 28−58.
(31) Müller-Plathe, F. Coarse-Graining in Polymer Simulation: From the Atomistic to the Mesoscopic Scale and Back. *ChemPhysChem* **2002**, *3* (9), 754−769.
(32) Vargas-Lara, F.; Douglas, J. F. Fiber Network Formation in Semi-Flexible Polymer Solutions: An Exploratory Computational Study. *Gels* **2018**, *4* (2), 27.
(33) Hall, D. M.; Grason, G. M. How geometric frustration shapes twisted fibres, inside and out: competing morphologies of chiral filament assembly. *Interface focus* **2017**, *7*, 20160140.
(34) Hall, D. M.; Bruss, I. R.; Barone, J. R.; Grason, G. M. Morphology Selection via Geometric Frustration in Chiral Filament Bundles. *Nat. Mater.* **2016**, *15*, 727−732.
(35) Wu, Z.; Beltran-Villegas, D. J.; Jayaraman, A. Development of a New Coarse-Grained Model to Simulate Assembly of Cellulose Chains Due to Hydrogen Bonding. *J. Chem. Theory Comput.* **2020**, *16* (7), 4599−4614.
(36) Jones, J. E. On the determination of molecular fields.−I. From the variation of the viscosity of a gas with temperature. *Proc. R. Soc. London, Ser. A* **1924**, *106* (738), 441.
(37) Weeks, J. D.; Chandler, D.; Andersen, H. C. Role of Repulsive Forces in Determining the Equilibrium Structure of Simple Liquids. *J. Chem. Phys.* **1971**, *54* (12), 5237−5247.
(38) Thompson, A. P.; Aktulga, H. M.; Berger, R.; Bolintineanu, D. S.; Brown, W. M.; Crozier, P. S.; in 't Veld, P. J.; Kohlmeyer, A.; Moore, S. G.; Nguyen, T. D.; et al. LAMMPS - a flexible simulation tool for particle-based materials modeling at the atomic, meso, and continuum scales. *Comput. Phys. Commun.* **2022**, *271*, 108171.
(39) Schneider, T.; Stoll, E. Molecular-dynamics study of a three-dimensional one-component model for distortive phase transitions. *Phys. Rev. B* **1978**, *17* (3), 1302−1322.
(40) Nishiyama, Y. Molecular interactions in nanocellulose assembly. *Philos. Trans. R. Soc., A* **2018**, *376* (2112), 20170047.
(41) Bergenstråhle, M.; Wohlert, J.; Himmel, M. E.; Brady, J. W. Simulation studies of the insolubility of cellulose. *Carbohydr. Res.* **2010**, *345* (14), 2060−2066. From NLM
(42) Cormen, T. H.; Leiserson, C. E.; Rivest, R. L.; Stein, C. *Introduction to Algorithms*, 3rd ed.; The MIT Press, 2009.
(43) Lott, J. R.; McAllister, J. W.; Arvidson, S. A.; Bates, F. S.; Lodge, T. P. Fibrillar Structure of Methylcellulose Hydrogels. *Biomacromolecules* **2013**, *14*, 2484−2488.
(44) Kobayashi, K.; Huang, C.; Lodge, T. P. Thermoreversible Gelation of Aqueous Methylcellulose Solutions. *Macromolecules* **1999**, *32*, 7070−7077.
(45) McAllister, J. W.; Schmidt, P. W.; Dorfman, K. D.; Lodge, T. P.; Bates, F. S. Thermodynamics of Aqueous Methylcellulose Solutions. *Macromolecules* **2015**, *48*, 7205−7215.
(46) Abraham, M. J.; Murtola, T.; Schulz, R.; Páll, S.; Smith, J. C.; Hess, B.; Lindahl, E. GROMACS: High performance molecular simulations through multi-level parallelism from laptops to supercomputers. *SoftwareX* **2015**, *1−2*, 19−25.
(47) Hansen, H. S.; Hünenberger, P. H. A Reoptimized GROMOS Force Field for Hexopyranose-Based Carbohydrates Accounting for the Relative Free Energies of Ring Conformers, Anomers, Epimers, Hydroxymethyl Rotamers, and Glycosidic Linkage Conformers. *J. Comput. Chem.* **2011**, *32*, 998−1032.
(48) Pol-Fachin, L.; Rusu, V. H.; Verli, H.; Lins, R. D. GROMOS 53A6GLYC, an Improved GROMOS Force Field for Hexopyranose-Based Carbohydrates. *J. Chem. Theory Comput.* **2012**, *8* (11), 4681−4690.
(49) Berendsen, H. J. C.; Grigera, J. R.; Straatsma, T. P. The missing term in effective pair potentials. *J. Phys. Chem.* **1987**, *91* (24), 6269−6271.
(50) Humphrey, W.; Dalke, A.; Schulten, K. VMD: Visual molecular dynamics. *J. Mol. Graphics Modell.* **1996**, *14* (1), 33−38.
(51) Gomes, T. C. F.; Skaf, M. S. Cellulose-Builder: A toolkit for building crystalline structures of cellulose. *J. Comput. Chem.* **2012**, *33* (14), 1338−1346.
(52) Nishiyama, Y.; Langan, P.; Chanzy, H. Crystal Structure and Hydrogen-Bonding System in Cellulose Iβ from Synchrotron X-ray and Neutron Fiber Diffraction. *J. Am. Chem. Soc.* **2002**, *124* (31), 9074−9082.
(53) Moon, R. J.; Martini, A.; Nairn, J.; Simonsen, J.; Youngblood, J. Cellulose nanomaterials review: structure, properties and nanocomposites. *Chem. Soc. Rev.* **2011**, *40* (7), 3941−3994.
(54) Abraham, M.; Alekseenko, A.; Bergh, C.; Blau, C.; Briand, E.; Doijade, M.; Fleischmann, S.; Gapsys, V.; Garg, G.; Gorelov, S.; et al. *GROMACS 2023.2*, 2023..
(55) Darden, T.; York, D.; Pedersen, L. Particle mesh Ewald: An $N\cdot\log(N)$ method for Ewald sums in large systems. *J. Chem. Phys.* **1993**, *98* (12), 10089−10092.
(56) Hess, B.; Bekker, H.; Berendsen, H. J. C.; Fraaije, J. G. E. M. LINCS: A Linear Constraint Solver for Molecular Simulations. *J. Comput. Chem.* **1997**, *18*, 1463−1472.
(57) Parrinello, M.; Rahman, A. Polymorphic Transitions in Single Crystals: A New Molecular Dynamics Method. *J. Appl. Phys.* **1981**, *52*, 7182−7190.
(58) Nosé, S. A Unified Formulation of the Constant Temperature Molecular Dynamics Methods. *J. Chem. Phys.* **1984**, *81*, 511−519.
(59) Aurenhammer, F. Voronoi diagrams—a survey of a fundamental geometric data structure. *ACM Comput. Surv.* **1991**, *23* (3), 345−405.
(60) Virtanen, P.; Gommers, R.; Oliphant, T. E.; Haberland, M.; Reddy, T.; Cournapeau, D.; Burovski, E.; Peterson, P.; Weckesser, W.; Bright, J.; et al. SciPy 1.0: fundamental algorithms for scientific computing in Python. *Nat. Methods* **2020**, *17* (3), 261−272.
(61) Lott, J. R.; McAllister, J. W.; Wasbrough, M.; Sammler, R. L.; Bates, F. S.; Lodge, T. P. Fibrillar Structure in Aqueous Methylcellulose Solutions and Gels. *Macromolecules* **2013**, *46*, 9760−9771.
(62) Morozova, S.; Schmidt, P. W.; Bates, F. S.; Lodge, T. P. Effect of Poly(ethylene glycol) Grafting Density on Methylcellulose Fibril Formation. *Macromolecules* **2018**, *51* (23), 9413−9421.
(63) Hynninen, V.; Hietala, S.; McKee, J. R.; Murtomäki, L.; Rojas, O. J.; Ikkala, O.; Nonappa. Inverse Thermoreversible Mechanical Stiffening and Birefringence in a Methylcellulose/Cellulose Nanocrystal Hydrogel. *Biomacromolecules* **2018**, *19*, 2795−2804.
(64) Hadden, J. A.; French, A. D.; Woods, R. J. Unraveling cellulose microfibrils: a twisted tale. *Biopolymers* **2013**, *99* (10), 746−756.
(65) Kannam, S. K.; Oehme, D. P.; Doblin, M. S.; Gidley, M. J.; Bacic, A.; Downton, M. T. Hydrogen bonds and twist in cellulose microfibrils. *Carbohydr. Polym.* **2017**, *175*, 433−439.
(66) Paavilainen, S.; Róg, T.; Vattulainen, I. Analysis of twisting of cellulose nanofibrils in atomistic molecular dynamics simulations. *J. Phys. Chem. B* **2011**, *115* (14), 3747−3755.
(67) Montoro, J. C. G.; Abascal, J. L. F. The Voronoi Polyhedra as Tools for Structure Determination in Simple Disordered-Systems. *J. Phys. Chem.* **1993**, *97* (16), 4211−4215.
(68) Grason, G. M. Chiral and achiral mechanisms of self-limiting assembly of twisted bundles. *Soft Matter* **2020**, *16* (4), 1102−1116.
(69) Grason, G. M.; Bruinsma, R. F. Chirality and Equilibrium Biopolymer Bundles. *Phys. Rev. Lett.* **2007**, *99* (9), 098101.
(70) Grason, G. M. Braided bundles and compact coils: The structure and thermodynamics of hexagonally packed chiral filament assemblies. *Phys. Rev. E* **2009**, *79* (4), 041919.

https://doi.org/10.1021/acs.biomac.3c01209
Biomacromolecules 2024, 25, 1682−1695